

Ab Initio Potential Energy Surfaces and
Quantum Dynamics of Rotational Inelastic Processes in the
 H^+ Collision with CS ($^1\Sigma^+$)

Rajwant Kaur and T. J. Dhillip Kumar*

Department of Chemistry

Indian Institute of Technology Ropar

Rupnagar 140001, India

(Dated: March 8, 2022)

Abstract

Rate coefficient for state-to-state rotational transitions in H^+ collision with CS has been obtained using accurate quantum dynamical close-coupling calculations to interpret microwave astronomical observations. Accurate three dimensional *ab initio* potential energy surfaces have been computed for the ground state and low-lying excited states of $\text{H}^+ - \text{CS}$ system using internally contracted MRCI method and aug-cc-pVQZ basis sets. Rotational excitation and deexcitation integral cross-sections are computed at low and ultra low collision energies, respectively. Resonances have been observed at very low energies typically below 50 cm^{-1} . Among all the transitions, $\Delta j=+1$ and $\Delta j=-1$ are found to be predominant for excitation and deexcitation, respectively. Deexcitation cross-section in the ultracold region is found to obey Wigner's threshold law. The magnitude of state-to-state excitation rate obtained is maximum for $j'=1$ in the temperature range 2–240 K while minimum for deexcitation in ultracold region. The rotational excitation cross-section obtained using vibrationally averaged potential show rotational rainbow maximum for $j'=2$ state. From simple unimolecular kinetics, the mean lifetime of rotationally excited CS trap is estimated to be 550 ns due to the H^+ collision at microkelvin temperature enabling precise spectroscopic measurement and studying molecular properties near quantum degeneracy.

*Electronic address: dhillip@iitrpr.ac.in

I. INTRODUCTION

Chemical processes in the interstellar medium occurring due to the ion-neutral collisions play a fundamental role in the areas of molecular physics and astrophysics. Proton collision with diatomic molecule is important in atmospheric chemistry and combustion processes. Various bound protonated molecular ions, such as H_3^+ , HCO^+ , HCS^+ , etc., have been identified in the interstellar medium through radio-astronomical spectra.^{1,2} Inelastic and charge transfer processes are responsible for the formation of these protonated ionic species. Many sulfur containing diatomic and polyatomic molecules have been detected in dense interstellar clouds. Among them, carbon monosulfide (CS) discovered in 1971 in the interstellar clouds and thioformyl cation, HCS^+ , detected in 1981 have attracted attention in understanding the sulfur chemistry of the interstellar clouds.^{3,4} CS is the first sulfur containing molecule detected in the interstellar space. It is a tracer gas in several regions of interstellar medium in our galaxy as well as in external galaxies. Collision of CS molecule with neutral species have been studied with most abundant molecules, He and H_2 .^{5,6} HCS^+ detection in dense interstellar clouds is due to large CS proton affinity and CS on reaction with protonated H_3^+ species favor HCS^+ formation.^{7,8}

Several chemical schemes have been proposed for the formation and dissociation of HCS^+ with its dissociative recombination mechanism and the results are validated by rate-coefficient calculations. Branching ratios and absolute cross-sections have been measured for the dissociative recombination of HCS^+ .⁹ Gerones *et al.* have analyzed the HCS^+ formation and its high stability over the range of photon energies.^{10,11} In the past *ab initio* studies have been performed to obtain the spectroscopic properties of HCS^+ with its optimized structural parameters.¹² Configuration interaction (CI) method with triple-zeta basis sets has been employed to study $\text{HCS}^+/\text{HSC}^+$ isomerization in 1985.¹³ In 1991, Talaty *et al.* reported that the HCS^+ isomer is linear and global minimum while its HSC^+ isomer is bent and higher in energy.¹⁴ Molecular properties, isomerization, and energetics of neutral CS, HCS/HSC and $\text{HCS}^+/\text{HSC}^+$ systems have been studied by Puzzarini.¹⁵ Cotton *et al.* have performed structural and spectroscopic studies of CS- HCS^+ van der Waals complex.¹⁶ The structural parameters, harmonic vibrational frequencies and charge distribution data of noble gas (Ng) inserted in the HCS^+ ion resulting in HNgCS^+ has been studied at

MP2, DFT and CCSD(T) level of methods.¹⁷ Recently, the time-dependent wave packet dynamics and charge transfer processes have been reported between the one-dimensional ground state (GS) and the low-lying excited states (ES) potential energy curves in collinear and perpendicular approaches of H towards CS⁺ at the MRCI/aug-cc-pVQZ level of theory.¹⁸

A kinetic study is important to understand the mechanisms and nature of molecule formation during collisions. Study of collisional rates of CS with H⁺ ion is important and still lacking. Interpretation of observed spectroscopic data by theoretical methods require kinetic models that include the study of rate coefficients and in turn, cross-sections of colliding species, H⁺ - CS. An isovalent and abundant species HCO⁺, has been explored for low-energy rotational inelastic transitions between H⁺ - CO (for $j \leq 4$)¹⁹ and H + CO⁺ (for $j \leq 8$)²⁰ with the computation of cross-sections and corresponding rate coefficient details. The study of HCS⁺ with its isovalent species, HCO⁺ and N₂H⁺, which are unique targets to explore the chemistry of molecular ions in protostellar shocks, has been done in the past to calculate the rate coefficients of the species in collision with He. Later, the abundance of HCS⁺ has been calculated using large velocity gradient approximation in radiative transfer code taking the collision rate coefficients calculated by Monteiro in 1984.^{21,22} Recently, Dubernet *et al.*²³ have studied the He-HCS⁺ system by computing their potential energy surface and inelastic rate coefficients for $j \leq 20$ in the temperature range 5 - 100 K and also compared the results of rate-coefficients computed previously.²¹ To the best of our knowledge, there are neither experimental study nor theoretical data available on inelastic low-energy rotational excitation and deexcitation of CS collisions with H⁺.

The analysis of observed spectra and estimation of abundance often requires collisional excitation and deexcitation rate coefficients. Quantum dynamics study of ion-neutral energy transfer process widens the understanding of kinetics of interstellar medium.²⁴ In addition, such collisions at very low energies by cooling to ultracold regime around 1 microkelvin temperatures are being investigated for precise spectroscopic measurements and to study the properties of molecular gases near quantum degeneracy.²⁵⁻²⁷ This will enable fundamental advance in quantum information processing and ultracold plasmas. The calculations of rotational excitation and deexcitation cross-sections and corresponding rate coefficients are performed for H⁺ - CS system. To investigate the collisions in the extreme

quantum regime where a single partial wave dominates the entire collision, the study of rotational inelastic excitation up to 800 cm^{-1} is extended to deexcitation transitions from 10^{-7} cm^{-1} to 5000 cm^{-1} for $j=5$ rotational level of CS.

The present work involves the collision study of H^+ with CS which require accurate potential energy surface (PES). The GS and the low-lying ES PESs of H^+ - CS system has been generated using *ab initio* method and the details are discussed in Sec. II. The multipolar expansion coefficients of potentials computed using rigid-rotor PES which is extracted from the full PES is described in Sec. III. Scattering details including the calculation of cross-sections and corresponding rate coefficients in the rigid-rotor approximation are provided in Sec. IV and the results obtained using vibrationally averaged potential are provided in Sec. V. Finally the summary of the present work is provided in Sec. VI.

II. AB INITIO POTENTIAL ENERGY SURFACES

Ab initio calculations have been performed for H^+ collision with CS in Jacobi coordinates to compute interaction potential, where variables R and r represent the distance of proton from center-of-mass of CS and interatomic distance of CS, respectively, and $\gamma = \cos^{-1}(R.r)$, is the angle between R and r as shown in Fig. 1. The method employed for the PES calcula-

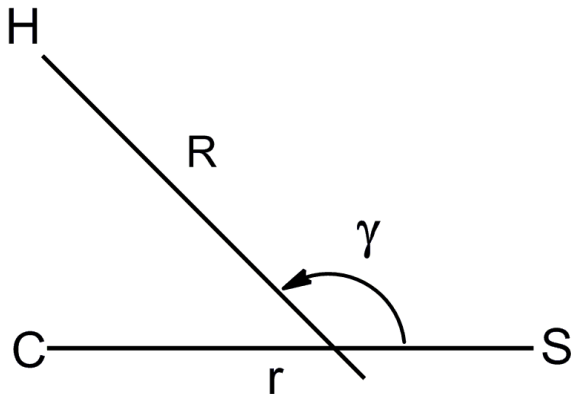


FIG. 1: Jacobi coordinates representation of H^+ collision with CS.

tion is internally contracted multireference configuration interaction (MRCI) as implemented in MOLPRO package.²⁸ The basis sets of Dunning's augmented correlation consistent polar-

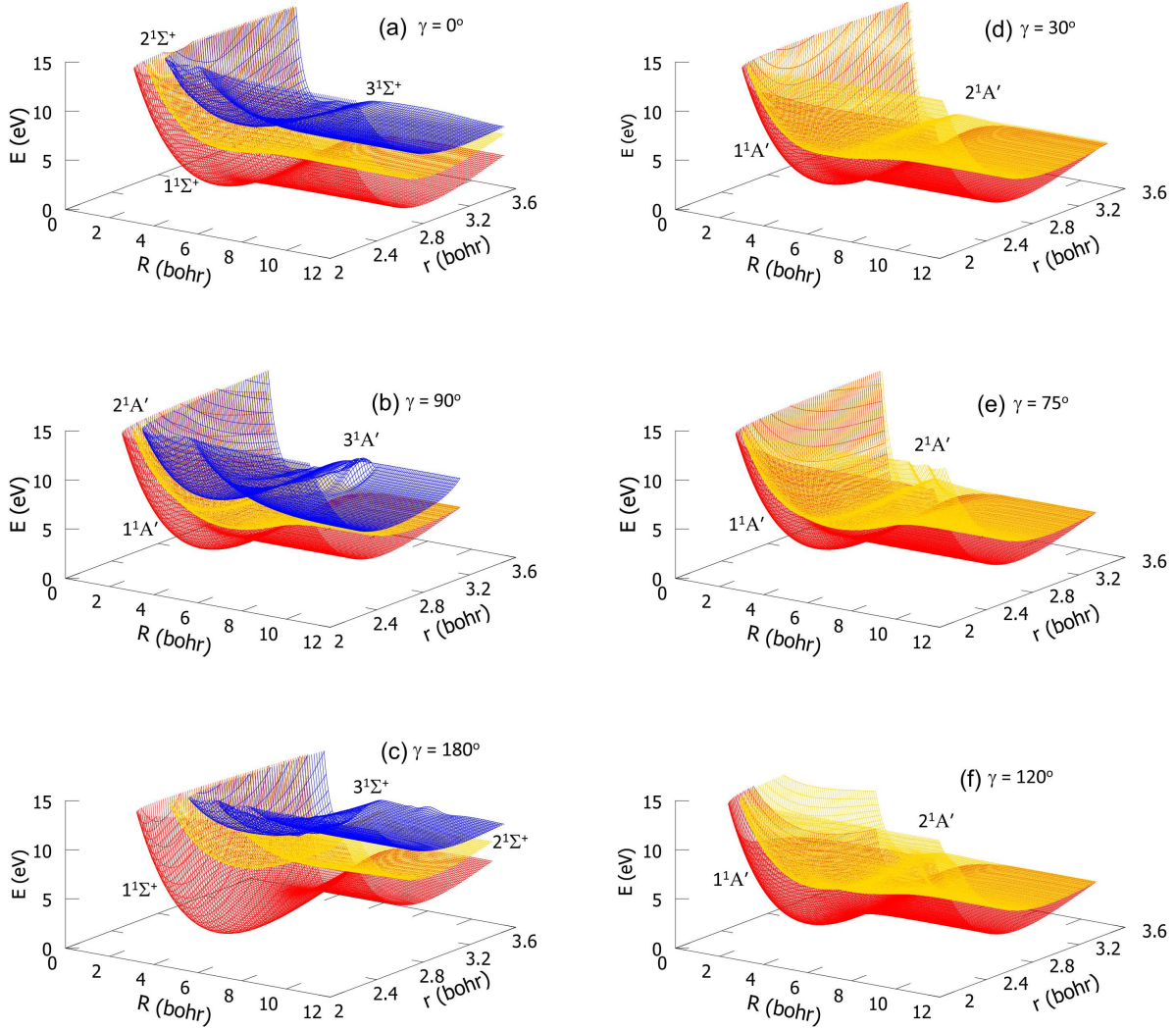


FIG. 2: The GS (red) and the low-lying ES (yellow, blue) PESs as a function of R and r at various orientations (γ).

ized quadruple zeta (aug-cc-pVQZ) for H, C and S atoms are chosen.²⁹ The adiabatic GS and the first ES PESs are computed for orientations $0^\circ \leq \gamma \leq 180^\circ$ with 15° increment. While the second ES PES is also computed for collinear ($\gamma=0^\circ, 180^\circ$) and perpendicular orientations ($\gamma=90^\circ$) as avoided crossings have been observed in one-dimensional PESs studied previously to investigate the non-adiabatic couplings present in the system using time-dependent wave packet dynamics.¹⁸ For the C_s point group, the computations employed 210 contracted functions with 133 in a' and 77 in a'' symmetry. The core orbitals having lowest 5 orbitals in a' and one orbital in a'' is kept frozen and are taken from self-consistent field calculations.

The active orbitals with 6-12 a' and 1-2 a'' symmetry incorporate remaining 10 electrons in the complete active space self-consistent field (CASSCF) calculations. The MRCI calculations following CASSCF method generate reference space of 1589 configurations: N, N-1 and N-2 internal configuration consist of 2907, 3139 and 2907 configurations, respectively. Total number of contracted configurations, 2436680 include 2744 internal, 864556 singly external and 1569380 doubly external configurations. The plots of computed PES as a function of R and r at fixed γ for 0° , 30° , 75° , 90° , 120° and 180° orientations are shown in Figs. 2(a)-(f) as reference. PESs are obtained with the set of grid points as follows: $R = 1.4-8.0(0.2)$ and $8.0-11.2(0.4) a_o$, $r=2.1-3.5(0.1) a_o$ and $\gamma = 0^\circ - 180^\circ(15^\circ)$. The $1-3 \ ^1\Sigma^+$ and $1-3 \ ^1A'$ electronic states are computed for collinear ($\gamma=0^\circ, 180^\circ$) and perpendicular orientation ($\gamma=90^\circ$), respectively, while $1-2 \ ^1A'$ electronic states are computed for angular (off-collinear) approaches. The numbers written in parenthesis implies the increment in the stated intervals. A total of 8190 *ab initio* points have been computed with the variation in R , r , γ being 42, 15, 13 points, respectively. The obtained adiabatic surfaces have been interpolated using cubic splines and shown in Figs. 2(a)-(f).

A. Analytical Fitting of GS Surface

The ground state potential energy surface has been fitted using the following analytical expression as a function of R and r at fixed values of γ :

$$V(R, r; \gamma) = \sum_{i=0}^7 \sum_{j=0}^{7-i} C_{ij} \left(\frac{1}{R}\right)^i \left(\frac{1}{r}\right)^j \quad (1)$$

The analytical fitting with the power series expansion in R and r has also been tried to represent zeroth order harmonic nature of CS vibration. Unfortunately, the function is not reproducing the potential at longer R and r values resulting in large error. Therefore, the inverse power expansion function has been tried which is reproducing the potential accurately with the standard deviation of the fit to be in the range of 0.5–4.8 meV for various γ orientations. The fitting coefficients, C_{ij} , for $\gamma = 0^\circ-180^\circ (15^\circ)$ are listed in Table S1 as supporting information.³⁰

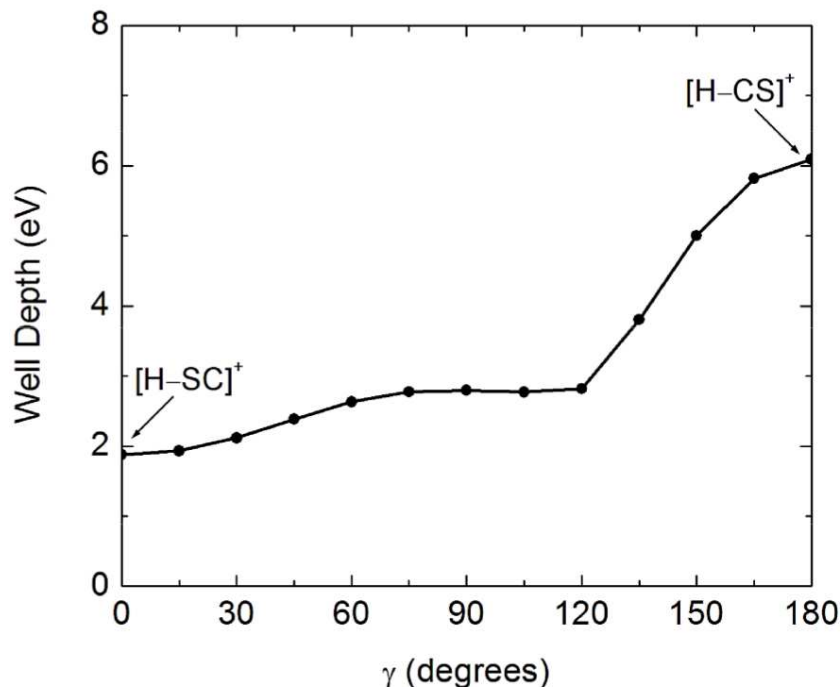


FIG. 3: Variation in the GS potential energy well in terms of well depth as a function of γ from 0° – 180° .

B. Stability of HCS^+ and HSC^+ Ions

From the computed *ab initio* surfaces the PES profile is generated by taking the difference of energy from minimum of the GS potential energy well to their corresponding asymptotic potential for every angle (γ). A plot with calculated well depths from HSC^+ ($\gamma=0^\circ$) to HCS^+ ($\gamma=180^\circ$), namely, from collinear through all the off-collinear arrangements in Fig. 3 is shown. As one can observe along the minimum at each γ , there is no barrier to the rotation of H from the S-end to the C-end of CS and the present results are validated with results reported by Bruna *et al.* in 1978.³¹ This makes the detection of HSC^+ isomer in the interstellar medium unreported till date due to small well-depth of 1.88 eV. Moreover, the linear HCS^+ is highly stable relative to its isomeric linear form HSC^+ by 4.21 eV (97 kcal/mol) whereas, this difference in energy reported earlier is 110 kcal/mol. This small energy difference between the present and the earlier reported value is due to the choice of method and basis sets. Present data can be taken as more reliable as larger basis sets are employed in the calculation. HCS^+ has the minimum energy compared to HSC^+ with dissociation energy of 6.09 eV.

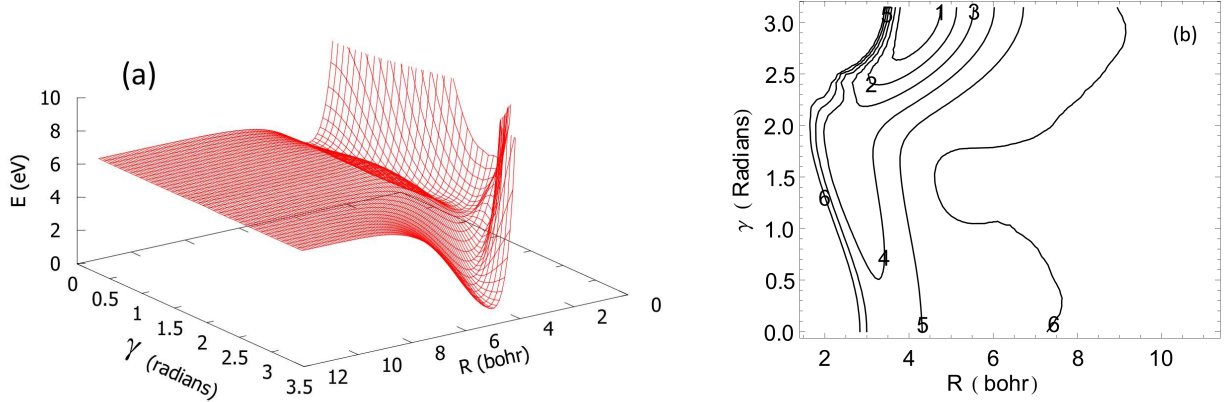


FIG. 4: (a) Rigid-rotor PES as a function of R and γ at fixed $r_{eq} = 2.900 a_o$ and (b) the contour plot of rigid-rotor surface of $H^+ - CS$ system.

III. SCATTERING STUDY IN RIGID-ROTOR SURFACE

For the scattering study, the rigid-rotor PES has been chosen with the CS bond distance fixed at an experimental equilibrium distance³² $r_{eq}=2.900 a_o$. In the present work the closed channel, $H^+ - CS$ ($^1\Sigma^+$), has been considered for scattering study although open channel, $H - CS^+$ ($^2\Sigma^+$), is also energetically accessible. The rigid-rotor PES is described as a function of R and γ at r_{eq} shown in Fig. 4(a). Two-dimensional contour plot of the surface is shown in Fig. 4(b). The numbers in the plot indicate the energy level of the contours in eV. From the plots, it can be seen that the global minimum, HCS^+ lies at $R = 4.0 a_o$ and $\gamma = 180^\circ$ (3.14 radians).

A. Asymptotic Potentials

Since the collision system is ionic, the asymptotic long-range potential will involve multipole moments which can be obtained at $r = r_{eq}$ as described below.

$$V_{as}(R, r_{eq}, \gamma) \approx \frac{\mu}{R^2} P_1(\cos\gamma) + \frac{Q}{R^3} P_2(\cos\gamma) - \frac{\alpha_0}{2R^4} - \frac{\alpha_2}{2R^4} P_2(\cos\gamma) + O(P_3) \quad (2)$$

where V_{as} is the asymptotic potential, μ, Q , are dipole, and quadrupole moments, respectively, and α_0 and α_2 are dipole polarizability components at r_{eq} . P 's denote the Legendre polynomials. The parameters, multipole moments and polarizability components at $r_{eq}=2.900 a_o$ are computed at the SCF and the MRCI level using MOLPRO package adopting Dunning's basis set of aug-cc-pVQZ. The computed values for $\mu = 0.785$ a.u., $Q =$

-1.820 a.u., $\alpha_0 = 36.996$ a.u. and $\alpha_2 = 23.878$ a.u. are used to obtain V_{as} . R is varied from 4.0–200.0 a_o for computing V_{as} (long-range interaction potential) and is merged with the *ab initio* PES (short-range interaction) available in the range of $R=1.4–11.2 a_o$ using cubic-spline interpolation method. This surface has been used for computing multipolar expansion coefficients.

B. Multi-Polar Expansion Coefficients

The rigid-rotor surface is fitted in the expansion of Legendre polynomials for scattering calculation as follows,

$$V(R, r = r_{eq}, \gamma) = \sum_{\lambda} V_{\lambda}(R) P_{\lambda}(\cos\gamma) \quad (3)$$

where, P_{λ} 's are the Legendre polynomial functions. The multipolar expansion coefficients are computed for $\lambda = 0$ to 12 and the plots of 13 computed values of V_{λ} as a function of R are shown in Fig. 5. It can be seen from Fig. 5(a) for $\lambda=0-5$ that V_0 and V_2 exhibit deep potential attractive wells. V_1 and V_3 display repulsive behavior with barriers. While V_4 has shallow well, V_5 show barrier-less repulsive behavior. The anisotropy of the interaction potential observed for V_{λ} , where $\lambda = 6-12$ is shown in Fig. 5(b). The magnitude of the coefficients decreases as the λ value increases. The coefficients obtained are interpolated using cubic spline method in the range of $R = 1.4–200 a_o$ for scattering study. The computed multipolar expansion coefficients indicate anisotropic nature of the rigid-rotor surface. The resulting V_{λ} 's are used for the kinetic study to compute various dynamical parameters such as integral and differential cross-sections, and rate-coefficients at low and ultracold collision energies. Tabulated values of V_{λ} fitting coefficients as a function of R are provided in Table S2 ($\lambda=0–5$) and Table S3 ($\lambda=6–12$) as supporting information.³⁰

IV. SCATTERING PHENOMENA: CLOSE-COUPLED CALCULATIONS

The effects of anisotropy in potentials can be well studied through rotational transition cross-sections. To obtain the cross-sections, time-independent coupled scattering equations are solved as implemented in the MOLSCAT code.^{33,34} Close-coupling method^{35,36} (CC) involve the solution of time-independent Schrödinger equation which compute the cross-

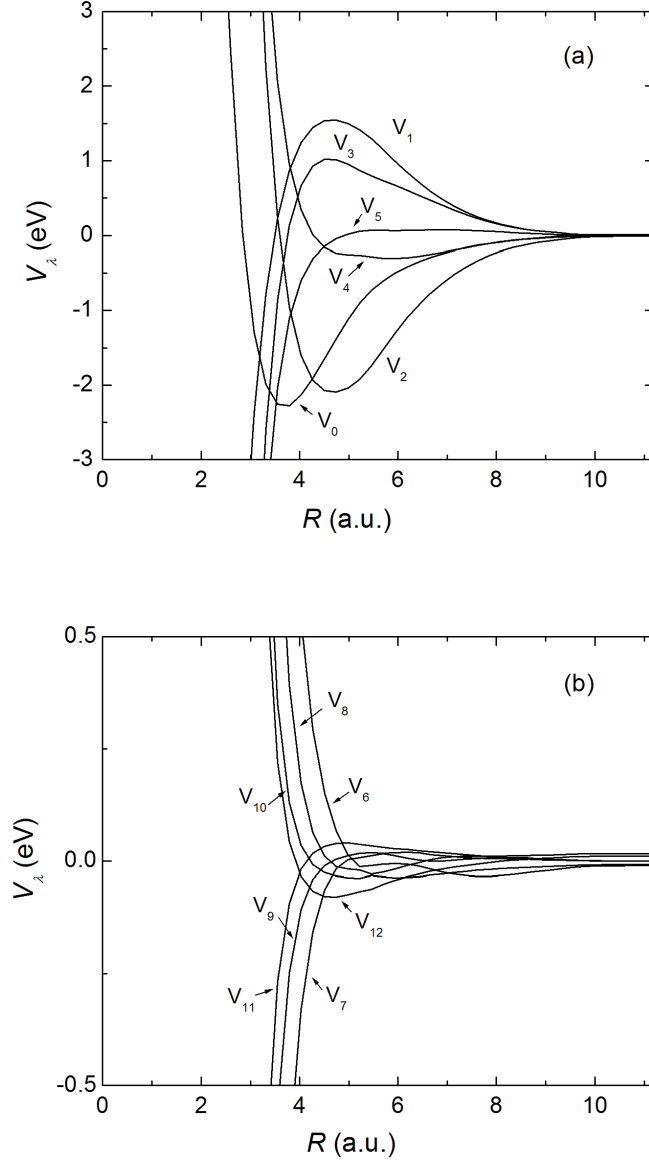


FIG. 5: Radial multipolar expansion coefficients for $\text{H}^+ - \text{CS}$ system as a function of R at $r = r_{eq}$ with (a) the lower coefficients $V_\lambda = 0$ to 5 and (b) the higher coefficients $\lambda = 6$ to 12. A few lower even coefficients show attractive wells while odd coefficients show repulsive behavior with barrier.

sections as

$$\sigma_{j \rightarrow j'}(E_j) = \frac{\pi}{k_j^2(2j+1)} \sum_{J=0}^{J+j} \sum_{l=|J-j|}^{J+j} \sum_{l'=|J-j|}^{J+j'} (2J+1) |\delta_{jj'} \delta_{ll'} - S_{jj'l}^J(E_j)|^2 \quad (4)$$

where total angular momentum $\mathbf{J} = \mathbf{1} + \mathbf{j}$ includes orbital angular momentum of complex and rotational angular momentum of the diatomic molecule. $k_j = \sqrt{2\mu E_j}/\hbar$ represents the

TABLE I: Parameters included in the MOLSCAT calculations for excitations.

Energy (cm ⁻¹)	No. of Open Channels	Total No. of Channels	Total Angular Momentum, J
20	5	20	80
50	8	23	100
80	10	25	120
100	11	26	150
200	16	29	200
300	19	32	280
800	31	35	700

wave vector for the incoming channel where E_j is center of mass kinetic energy and $S_{jj'lv}$ is the scattering S -matrix.

The inelastic differential cross-sections can be computed using,

$$\frac{d\sigma_{j \rightarrow j'}}{d\omega} = \frac{1}{(2j+1)k_j^2} \sum_{m,m'} \left| \sum_{l'} (2l'+1) \left[\frac{(l' - |m - m'|)!}{(l' + |m - m'|)!} \right]^{1/2} A_{(jm \rightarrow j'm')}^{l'} P_{l'}^{|m-m'|}(\cos \theta) \right|^2 \quad (5)$$

in the center-of-mass of the system in which the initial and final wave vectors, k_j and $k_{j'}$, are related via $\cos \theta = k_j \cdot k_{j'}$. The partial amplitude $A_{(jm \rightarrow j'm')}^{l'}$ is related to transition matrix, $T_{jl \rightarrow j'l'}^J$ which in turn is related to scattering S -matrix.

The rate coefficients are calculated by averaging the obtained cross-sections over a Boltzmann distribution of kinetic energy

$$k_{j \rightarrow j'}(T) = \sqrt{\frac{8k_B T}{\pi \mu}} \left(\frac{1}{k_B T} \right)^2 \int_0^\infty \sigma(E_j) E_j \exp\left(\frac{-E_j}{k_B T}\right) dE_j \quad (6)$$

where k_B is the Boltzmann constant and μ is the reduced mass of the system.

A. State-to-State Excitation Cross-sections and Rate Coefficients

Reliable close-coupling method is used to compute the cross-sections in the energy range of 2–800 cm⁻¹ employing the diabatic modified log-derivative method of Manolopoulos for

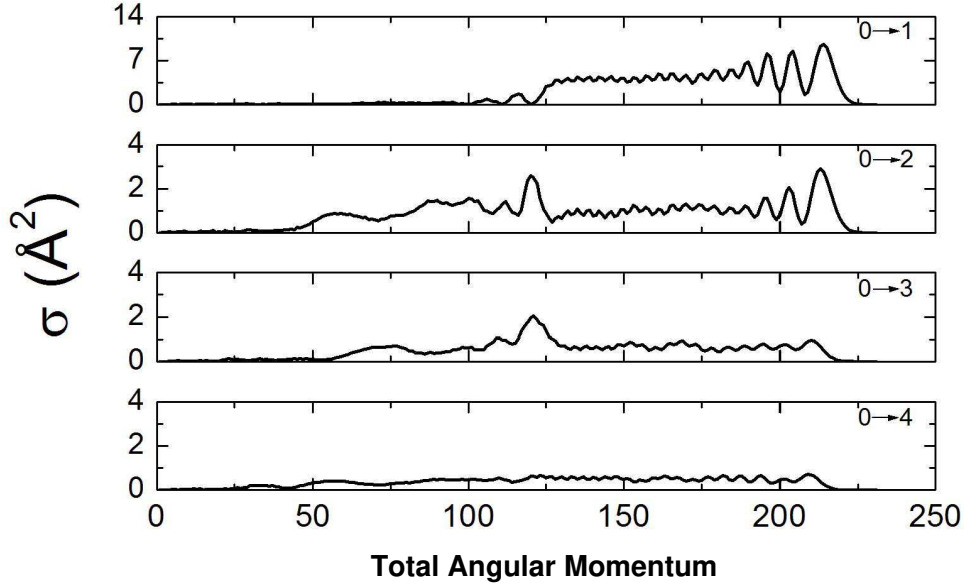


FIG. 6: Computed partial opacities for state-to-state inelastic cross-sections as a function of total angular momentum for the CC calculation at $E = 300 \text{ cm}^{-1}$.

radial integration of coupled channel equations.³⁷ The input parameters in the calculation are taken as, CS rotational constant, $B_e = 0.81923 \text{ cm}^{-1}$ and reduced mass of the system, μ , being 0.985 a.u. with values of R_{min} and R_{max} as 1.4 and $100 a_0$, respectively. The CC calculations have been performed from an energy value corresponding to the opening of the lowest inelastic channel to a total energy of 800 cm^{-1} . The energy range has been carefully spanned to observe the presence of resonances due to quasi-bound states supported by the attractive part of the interaction potential. The energy steps are 0.1 cm^{-1} below 40 cm^{-1} , 1 cm^{-1} from 40 to 100 cm^{-1} , 20 cm^{-1} from 100 to 400 cm^{-1} , and 100 cm^{-1} from 400 to 800 cm^{-1} . Minimum 13 closed channels are included at each collision energy up to 300 cm^{-1} to ensure convergence of cross-section. Maximum value of rotational quantum number taken is 35 at $E = 800 \text{ cm}^{-1}$. Steps parameter is kept at 30 up to 100 cm^{-1} and at 10 for energies above 100 cm^{-1} . Cross-sections as a function of number of closed channels for $j=0$ to $j'=1$ excitation at different energies is shown in Fig. S1 of supporting information.³⁰ Also, convergence of cross-sections are achieved through sufficient number of partial waves or total angular momentum. To test the convergence, inelastic opacities

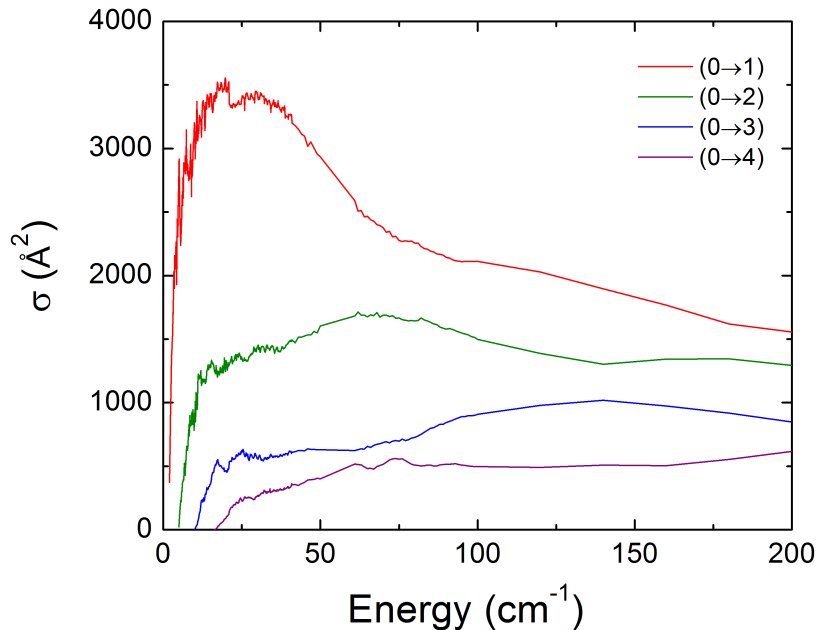


FIG. 7: Computed state-to-state integral cross-section for excitations from $j=0 \rightarrow j'=1, 2, 3, 4$ using the CC method up to $E = 200 \text{ cm}^{-1}$.

have been computed for the lowest four channels as a function of total angular momentum and shown for the collision energy $E=300 \text{ cm}^{-1}$ in Fig. 6. The magnitude of opacity is quite large for $(0 \rightarrow 1)$ transition and it decreases in the order from $(0 \rightarrow 2)$, $(0 \rightarrow 3)$ and $(0 \rightarrow 4)$. The convergence is ensured at values of angular momentum (maximum) of 280 when the collision energy is 300 cm^{-1} . The parameters used in the calculation are provided in the Table I. The calculations are performed using parallel code³⁴ of MOLSCAT for energies above 400 cm^{-1} .

Full close-coupling calculations have been performed at low energies ($2\text{--}800 \text{ cm}^{-1}$) and Fig. 7 displays the variation of calculated rotationally inelastic excitation cross-sections ($\sigma_{j \rightarrow j'}$) as a function of collision energy up to 200 cm^{-1} . The rotational excitations computed are plotted for $j=0 \rightarrow j' = 1\text{--}4$. Close examination of the cross-sections at low energies typically below 50 cm^{-1} show resonances. The cross-sections oscillate at low energies attaining maximum while with the increase of energy the magnitude of cross-sections decreases and plateau is reached. Maximum value of cross-section is found

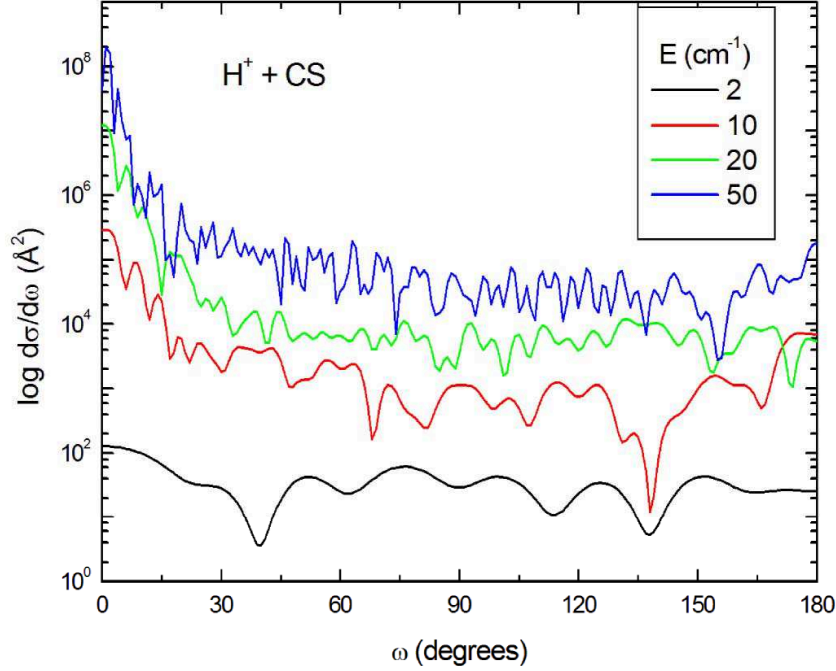


FIG. 8: Differential cross-sections for $j = 0 \rightarrow j' = 1$ excitation at the range of collision energies below 50 cm^{-1} .

in the transition from $j = 0 \rightarrow j' = 1$, which decreases for higher rotational energy levels in the order of $j = 0 \rightarrow j' = 2-4$. For all the excitations, cross-sections follow the similar behavior. The calculations involving close coupling method for excitations are performed with energy restricted up to 800 cm^{-1} as convergence of cross-sections put limitation with the increase of open channels and value of total angular momentum. This is due to collision energy increase, the number of j levels coupled by the potential increases and the number of close-coupling equations to be solved become very large.

The CC S -matrices obtained from MOLSCAT are used to compute state-to-state differential cross-sections, $d\sigma/d\omega$, at intervals of 1° using the Eq. (5). The results are shown in Fig. 8 which shows the angular scattering for the transitions $j = 0$ to $j' = 1$ at different energy values, namely, $E = 2, 10, 20$ and 50 cm^{-1} . For clarity, the differential cross-sections at increasing energies have been shifted by one order of magnitude higher correspondingly.

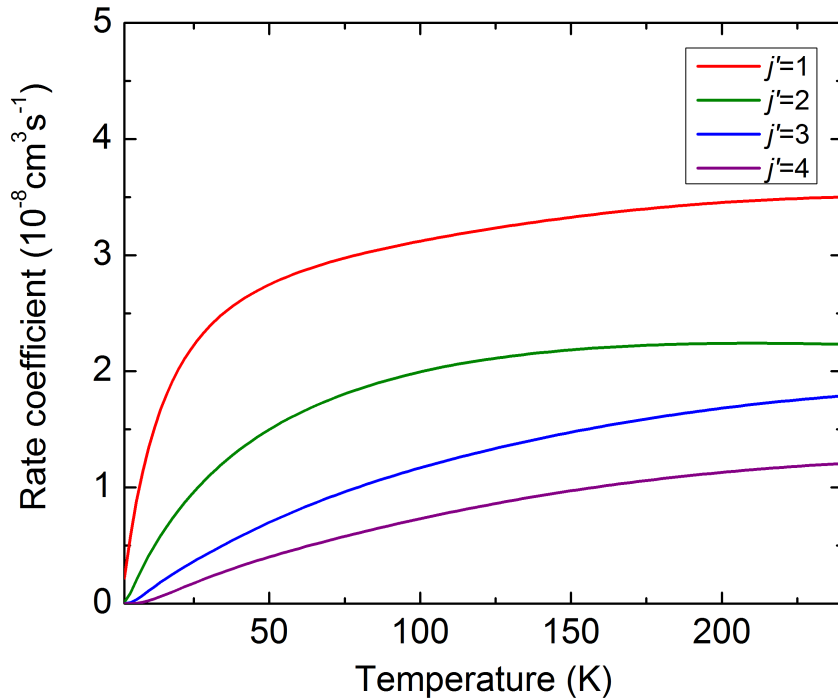


FIG. 9: Computed state-to-state rate-coefficient for excitation from $j=0 \rightarrow j'=1, 2, 3, 4$ using the CC method.

It is evident from the figure that the oscillations in the differential cross-section is less at lower energy while it gradually increases attaining maximum at 50 cm^{-1} .

The values of the cross-section allow one to calculate rate-coefficients as function of temperature using the Eq. (6). The state-to-state rate coefficients are computed for rotational transitions over a range of temperatures up to 240 K as shown in Fig. 9. The rates are higher for $(0 \rightarrow 1)$ transitions similar to cross sections and decreases for other higher excitations. In the spanned range of temperatures, rates are found to be large in magnitude for $(0 \rightarrow 1)$. $(0 \rightarrow 2)$ excitation rate is found to be two-third in magnitude of $(0 \rightarrow 1)$ while $(0 \rightarrow 2)$ rate is one-half of $(0 \rightarrow 1)$ magnitude.

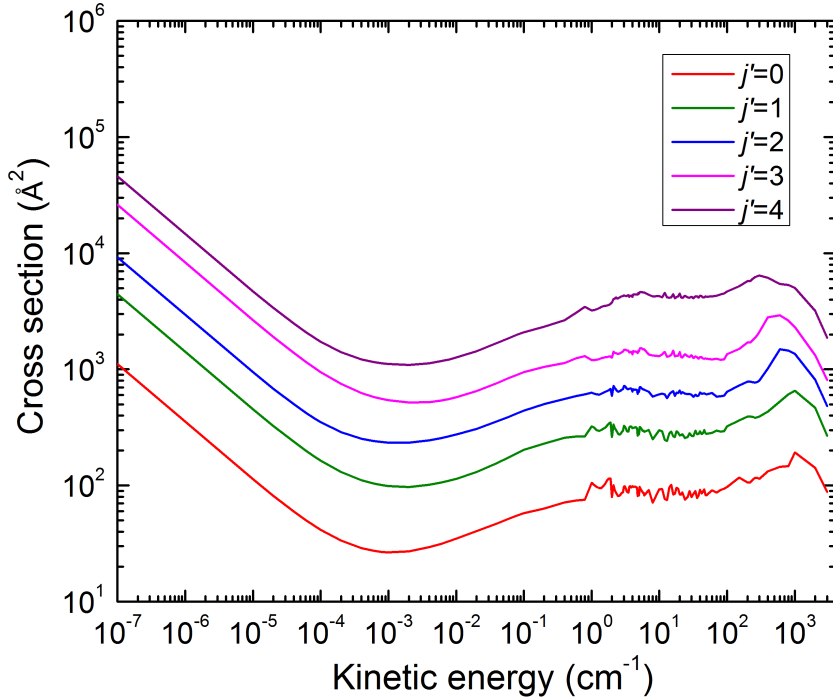


FIG. 10: Deexcitation cross-sections as a function of kinetic energy for $j=5 \rightarrow j'=0, 1, 2, 3, 4$ transitions.

B. State-to-State Deexcitation Cross-Sections and Rate Coefficients

State-to-state cross-sections have been obtained for rotational deexcitation of CS molecule for initial level of $j=5$ to final lower rotational levels $j'=0, 1, 2, 3, 4$. The CC method is computationally expensive for higher energies and the coupled state approximation method results does not overlap with the CC result in this system. Therefore, state-to-state deexcitation cross-sections have been calculated up to 5000 cm^{-1} using the CC method. For the computation of cross-sections at ultra low energies from 10^{-7} cm^{-1} the logarithmic energy grid has been used. The hybrid modified log-derivative Airy propagator of Alexander and Manolopoulos³⁸ which uses the diabatic modified log-derivative method at short range, while changes to the Airy propagator at long range is employed. For the ultra-cold collision regime, R_{max} is extended up to $200 a_o$ with $R_{mid}=110 a_o$ with 30 as steps parameter in the input. Deexcitation cross-section from kinetic energy 10^{-7} cm^{-1} to

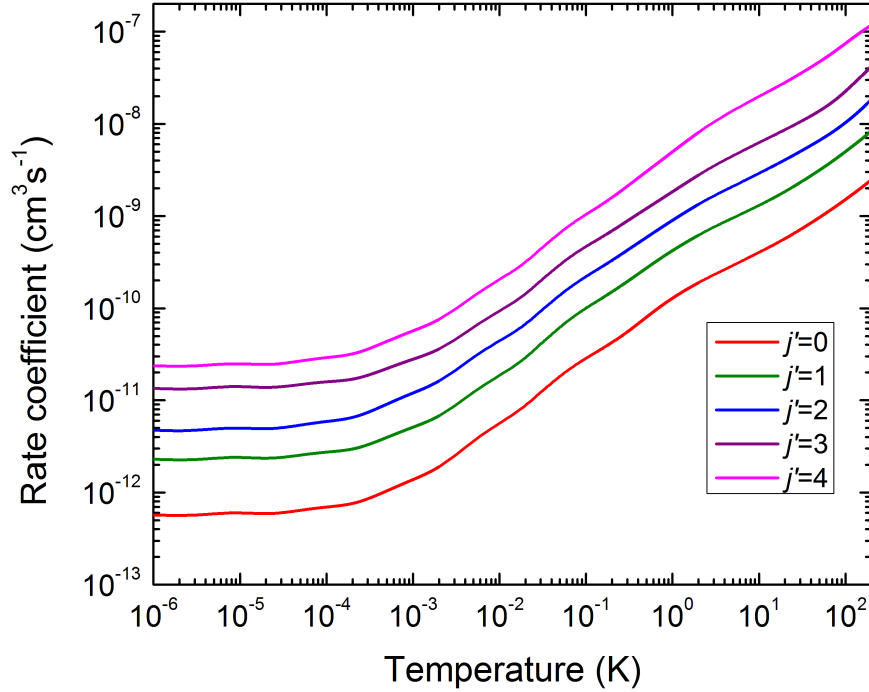


FIG. 11: Deexcitation rate coefficients as a function of temperature for $j=5 \rightarrow j'=0, 1, 2, 3, 4$ transitions.

$5 \times 10^3 \text{ cm}^{-1}$ for $j = 5$ to $j' = 4-0$ has been computed as a function of kinetic energy and shown in Fig. 10. Parallel code³⁴ of MOLSCAT has been used to compute cross-sections for the collision energy range of $400 \text{ cm}^{-1} - 5000 \text{ cm}^{-1}$. It is observed that $\Delta j = -1$ dominates rotational quenching from higher rotational level to all lower possible rotational energy levels. With the increase of j' , the magnitude of cross-section increases and it is maximum for $j' = 4$. Resonances are seen in the energy range from $2-50 \text{ cm}^{-1}$ and these gets suppressed with increasing rotational energy levels. In the ultra low energy regime, the cross-section is found to vary inversely to the velocity below 10^{-4} cm^{-1} . This behavior is in accordance as predicted by Wigner threshold laws³⁹ at ultra-low collision energies where only the s -wave scattering contributes and the cross-section vary inversely with the relative velocity. The deexcitation cross-sections decrease to a minimum near 10^{-3} cm^{-1} and then increases to reach maximum at 10^{-7} cm^{-1} .

The rotational quenching rate-coefficients for $j=5 \rightarrow j'=4-0$ as a function of temperature have been obtained by averaging the cross-section over Boltzmann distribution of kinetic energy and shown in Fig. 11. The temperature is varied from 10^{-6} K to 200 K. The collision rates found to be low and constant up to 10^{-4} K then increases gradually with increasing temperature for all transitions. The deexcitation rate from $j = 5$ to $j' = 4$ is found to be maximum and decreases gradually for each j' level with the lowest for $j'=0$. This shows that $\Delta j=-1$ transition is dominant among all. The reported state-to-state rate coefficients for collisional excitation and deexcitation will help in describing dynamics of energy transfer process and interpretation of microwave observations of the interstellar gas. To our knowledge, unfortunately, there has been no experimental data available of rate coefficient for rotational transitions of CS- H^+ collision system. It is presumed that in future the availability of experimental data will give credence the theoretical reported rate coefficients.

In the ultracold temperature region, total deexcitation rate coefficient is found to be $1.8 \times 10^{-09} \text{ cm}^3 \text{ s}^{-1}$ for the initial $j=5$ state. From the total deexcitation rate coefficient the mean lifetime (τ) of the rotational excited state of the CS in the H^+ environment has been estimated. A qualitative estimate of the typical quenching lifetime expected under trap condition can be obtained from the simple unimolecular kinetic equation,

$$\frac{d}{dt}N^{(CS)^*}(t) = -\lambda N^{(CS)^*}(t) \quad (7)$$

where $N^{(CS)^*}(t)$ is the number density of the excited rotational states of the CS molecule present at time t , $\lambda = k(T).N_0^{H^+}$ describe an effective unimolecular decay rate, $k(T)$ is effective temperature-dependent quenching rate coefficient, $N_0^{H^+}$ is the H^+ number density.⁴⁰ The mean lifetime of CS present in the trap is then given by $\tau = 1/\lambda = 1/(k(T).N_0^{H^+})$. Assuming a typical number density of $H^+ = 10^{16} \text{ cm}^{-3}$ and at ultracold temperature in the range of microK with $k = 1.8 \times 10^{-09} \text{ cm}^3 \text{ s}^{-1}$ for initial $j = 5$ state, the mean lifetime, τ , of a typical rotationally excited state CS in the trap will be 550 ns, a time interval which corresponds to an effective decay rate, λ , $1.8 \times 10^7 \text{ s}^{-1}$. To our knowledge, there is no rate coefficient data reported for rotational transitions taking place ranging from ultracold to low energy regions of H^+ collision with CS molecule. In addition, the life-time and decay rate data obtained at the ultracold region will help to arrive at precise spectroscopic

measurements and to study the properties of molecular gases near quantum degeneracy.

V. SCATTERING STUDY IN VIBRATIONALLY AVERAGED POTENTIAL

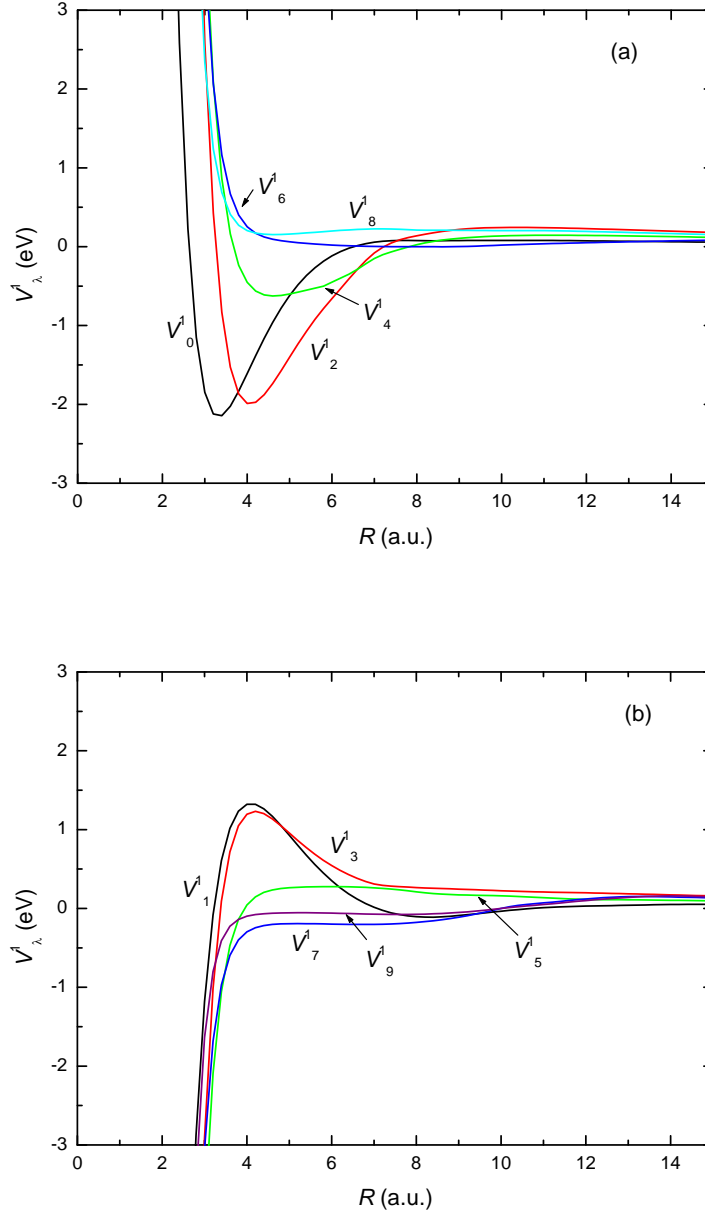


FIG. 12: Radial multipolar expansion coefficients for vibrationally averaged potential as a function of R with (a) the even and (b) odd coefficients.

The rotational excitation cross-section using vibrationally averaged potential have been

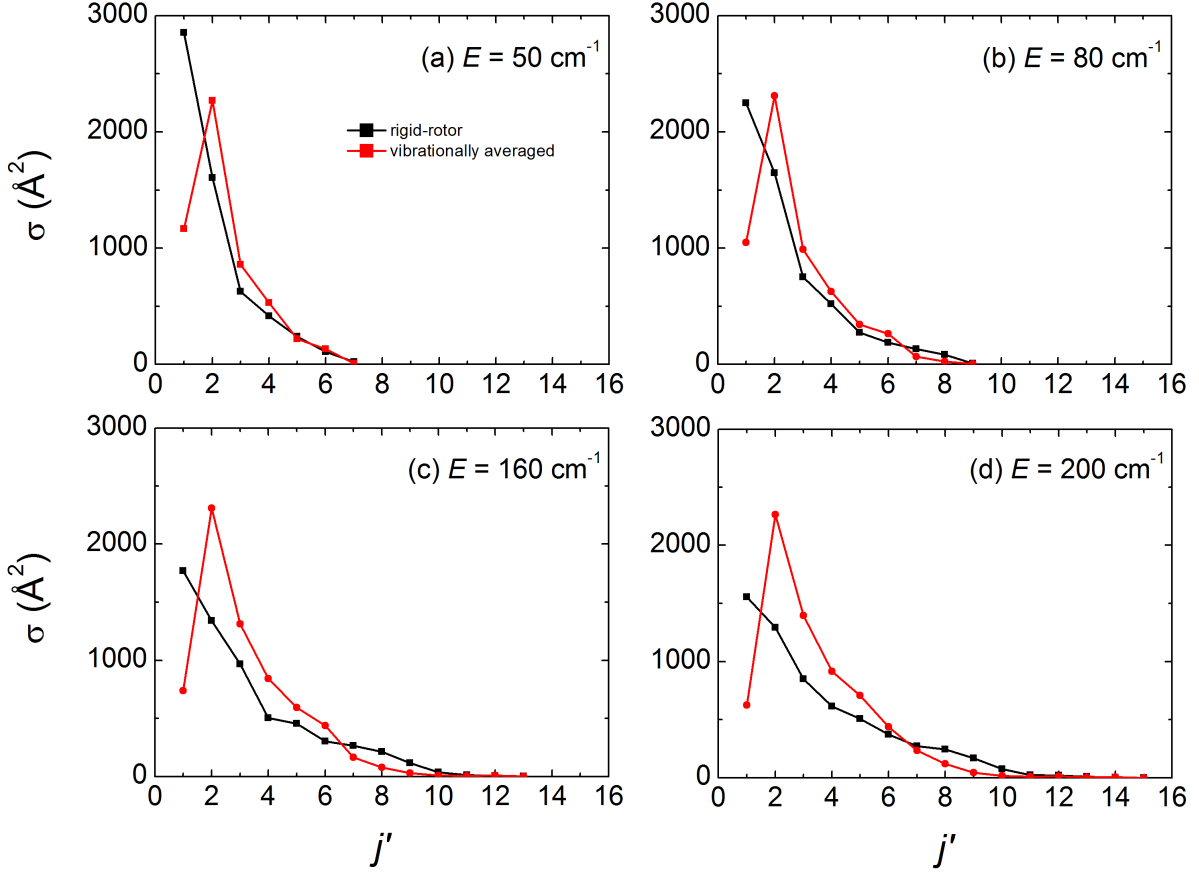


FIG. 13: Comparison of the computed integral cross-sections for rigid-rotor potential and vibrationally averaged potential into all allowed values of j' at $E =$ (a) 50 cm^{-1} , (b) 80 cm^{-1} , (c) 160 cm^{-1} and (d) 200 cm^{-1}

calculated for the system. The vibrationally averaged potentials have been obtained using the corresponding vibrational wavefunctions as shown below:

$$V^1(R; \gamma) = \langle \psi_v | V(R, r; \gamma) | \psi_v \rangle, \quad (8)$$

where V^1 defines the averaged potential obtained for vibrational state v , with the vibrational wavefunction, ψ_v . The anisotropy of V^1 obtained is analyzed in terms of multipolar expansion coefficients, V_λ^1 , obtained using Eq. (3) and shown as a function of R in Fig. 12. Vibrationally averaged V_λ^1 terms are similar from those obtained by employing the rigid-rotor potential V_λ at $r = r_{eq}$. $V_0^1 - V_5^1$ are strong in magnitude and

their characteristics are almost similar to the rigid-rotor V_λ 's as shown in the figure. However, V_1^1 and V_3^1 terms shows repulsive maximum at larger radial distance with centrifugal barrier and becomes attractive by crossing the radial axis at shorter R values. Higher V_λ^1 potentials exhibit similar behaviour at larger radial distances as observed for the rigid-rotor V_λ potentials. Tabulated values of V_λ^1 fitting coefficients as a function of R are provided in Table S4 ($\lambda=0-5$) and Table S5 ($\lambda=6-12$) as supporting information.³⁰

The integral cross-section has been computed using vibrationally averaged potential V_λ^1 under CC scheme at the collision energies, $E=50, 80, 160$ and 200 cm^{-1} and shown in Fig. 13 as a function of j' . For comparison, the cross-sections computed using rigid-rotor potential is also shown. The rotational cross-sections computed using V_λ^1 potential at various energies is found to be larger in magnitude as compared to those obtained from using the rigid-rotor potential, V_λ , for the lower j' states and merging together for higher j' 's states. Rotational rainbow maximum is observed at $j'=2$ for the cross-sections computed at various collision energies using vibrationally averaged potentials.^{41,42}

VI. SUMMARY AND CONCLUSIONS

Ab initio full PESs of H^+ -CS system have been generated using the MRCI/aug-cc-pVQZ method. The GS PES computed for various angular orientations reveals the stable configuration of linear HCS^+ with dissociation energy of 6.09 eV. Potential energy profile of the system displays the barrier-less rotation of H from the S-end to the C-end of CS. Multipolar expansion coefficients computed from the surface indicate anisotropic nature of the system. Inelastic rotational excitations and deexcitations have been studied in the H^+ - CS system in the GS at low energy ($2-800 \text{ cm}^{-1}$) and ultra-low energy (10^{-7} to $5 \times 10^3 \text{ cm}^{-1}$) regime on the rigid rotor PES extracted from the full PES at $r_{eq}=2.900 a_o$. Cross-sections are computed for inelastic rotational transitions using the CC method. The rotational transitions favor $\Delta j=+1$ and -1 for excitation and deexcitation, respectively. Wigner's threshold law is obeyed for energies less than 10^{-4} cm^{-1} where the magnitude of cross-section increases as the collision energy in ultracold region is decreased. Rate coefficients calculated for range of energies will help in interpretation of rates of formation and decomposition of astronomical species. Scattering dynamics has been performed using vibrationally averaged potential of

CS molecule. The anisotropy for the vibrationally averaged potential has been analyzed in terms of multipolar expansion coefficients. The rotational cross-sections obtained using vibrationally averaged potential showed rotational rainbow maximum for $j'=2$ state. An estimate of mean lifetime of the trapped CS due to H^+ collision in microkelvin region is found to be very long time (550 ns) which will allow precise spectroscopic measurement and to study the properties of molecular gases near quantum degeneracy.

ACKNOWLEDGEMENTS

This research is supported by the Department of Science and Technology, New Delhi (DST Grant No. EMR/2014/000017). Kaur acknowledges IIT Ropar for research fellowship. The calculations are carried out in IIT Ropar High-Performance Computing cluster facility.

-
- [1] E. Herbst, Chem. Soc. Rev. **30**, 168 (2001).
- [2] S. L. W. Weaver, D.E. Woon, B. Ruscic and B. J. McCall, Astrophys. J. **697**, 601 (2009).
- [3] A. A. Penzias, P. M. Solomon, R. W. Wilson and K. B. Jefferts, Astrophys. J. **168**, L53 (1971).
- [4] P. Thaddeus, M. Guelin and R. A. Linke, Astrophys. J. **246**, L41 (1981).
- [5] F. Lique, F., A. Spielfiedel and J. Cernicharo, Astron. Astrophys. **451**, 1125 (2006).
- [6] O. D. Alpizar, T. Stoecklin, P. Halvick and M. L. Dubernet, J. Chem. Phys. **139**, 204304 (2013).
- [7] T. McAllister, Astrophys. J. **225**, 857 (1978).
- [8] T. J. Millar, N. G. Adams, D. Smith and D. C. Clary, Mon. Not. R. Astron. Soc. **216**, 1025 (1985).
- [9] H. Montaigne, W.D. Geppert, J. Semaniak, F. Österdahl, et al., Astrophys. J. **631**, 653 (2005).
- [10] M. Gerones, M. F. Erben, R. M. Romano, R. L. C. Filho and C. O. D. Vedova, J. Phys. Chem. A **114**, 12353 (2010).
- [11] M. Gerones, M. F. Erben, R. M. Romano, R. L. C. Filho and C. O. D. Vedova, J. Phys. Chem. A **116**, 2571 (2012).
- [12] P. Botschwina and P. Sebald, J. Mol. Spectrosc. **110**, 1 (1985).
- [13] S. A. Pope, I. H. Hillier and M. F. Guest, J. Am. Chem. Soc. **107**, 3789 (1985).
- [14] E. R. Talaty, Y. Huang and M. E. Zandler, J. Am. Chem. Soc. **113**, 779 (1991).
- [15] C. Puzzarini, J. Chem. Phys. **123**, 024313 (2005).
- [16] C. E. Cotton, J. S. Francisco, R. Linguerrri and A. O. Mitrushchenkov, J. Chem. Phys. **136**, 184307 (2012).
- [17] A. Ghosh, D. Manna and T. K. Ghanty, J. Phys. Chem. A **119**, 2233 (2015).
- [18] R. Kaur and T. J. D. Kumar, Mol. Phys. **113**, 3271 (2015).
- [19] T. J. D. Kumar and S. Kumar, J. Chem. Phys. **124**, 034314 (2012).
- [20] S. Andersson, G. Barinovs and G. Nyman, Astrophys. **678** 1042, (2008).
- [21] T. Monteiro, Mon. Nor. R. Astron. Soc. **210**, 1 (1984).
- [22] L. B. Podio, C. Lefloch, C. Ceccarelli, C. Codella and R. Bachiller, A & A, **565**, A64 (2014).
- [23] M. L. Dubernet, E. Q. Sanchez and P. Tuckey, J. Chem. Phys. **143**, 044315 (2015).

- [24] E. Bodo, *Physica Scripta*. **80**, 048117 (2009).
- [25] P. F. Staantum, K. Hojbjerre, P. S. Skyt, A. K. Hansen and M. Drewsen, *Nature Phys.* **6**, 271 (2010).
- [26] M. T. Bell and T. P. Softley, *Mol. Phys.* **107**, 99 (2009).
- [27] B. Yang, P. Zhang, X. Wang, P. C. Stancil, J. M. Bowman, N. Balakrishnan and R. Forrey, *Nature Comm.* **6**, 6629 (2015).
- [28] H.-J. Werner, P. J. Knowles, G. Knizia, F. R. Manby, M. Schütz, P. Celani, T. Korona, R. Lindh, A. Mitrushenkov, G. Rauhut, K. R. Shamasundar, T. B. Adler, R. D. Amos, A. Bernhardsson, A. Berning, D. L. Cooper, M. J. O. Deegan, A. J. Dobbyn, F. Eckert, E. Goll, C. Hampel, A. Hesselmann, G. Hetzer, T. Hrenar, G. Jansen, C. Köppl, Y. Liu, A. W. Lloyd, R. A. Mata, A. J. May, S. J. McNicholas, W. Meyer, M. E. Mura, A. Nicklass, D. P. O’Neill, P. Palmieri, D. Peng, K. Pflüger, R. Pitzer, M. Reiher, T. Shiozaki, H. Stoll, A. J. Stone, R. Tarroni, T. Thorsteinsson, M. Wang, MOLPRO, version 2012.1, a package of *ab initio* programs 2012, see <http://www.molpro.net>.
- [29] T. H. Dunning, *J. Chem. Phys.* **90**, 1007 (1989).
- [30] See Supplementary Material Document No. for the cross-sections as a function of number of closed channels for $\gamma = 0^\circ - 180^\circ$ (15°) is shown in Fig. S1. The tabulated C_{ij} fitting coefficients in Table S1, V_λ coefficients in Tables S2-S3 and V_λ^1 coefficients in Tables S4-S5 are provided in the EPAPS.
- [31] P. J. Bruna, S. D. Peyerimhoff and R. Buenker, *J. Chem. Phys.* **27**, 33 (1978).
- [32] K. P. Huber, G. Herzberg, *Constants of diatomic molecules*, Van Nostrand, New York, 1979.
- [33] J. Hutson, S. Green, MOLSCAT computer code, version 14, Collaborative Computational Project No. 6 of the Science and Engineering Research Council, United Kingdom, 1994.
- [34] G. C. McBane, "PMP MOLSCAT" a parallel version of Molscat version 14 available at <http://faculty.gvsu.edu/mcbaneg/pmpmolscat>, Grand Valley State University (2005).
- [35] A. M. Arthurs and A. Dalgarno, *Proc. R. Soc. London, Ser. A* **256**, 540 (1960).
- [36] F. A. Gianturco, *The Transfer of Molecular Energies by Collisions* (Springer, Berlin, 1979).
- [37] D. E. Manolopoulos, *J. Chem. Phys.* **85**, 6425 (1986).
- [38] M. H. Alexander and D. E. Manolopoulos, *J. Chem. Phys.* **86**, 2044 (1987).
- [39] E. P. Wigner, *Phys. Rev.* **73**, 1002 (1948).
- [40] M. Tacconi, F. A. Gianturco, E. Yurtsever and D. Caruso, *Phys. Rev. A* **84**, 013412 (2011).

- [41] R. Schinke, H. Jorsch and D. J. Poppee, *Chem. Phys* **77**, 6005 (1982).
- [42] M. Baer, *Molecular Collision Dynamics* (Springer, Berlin, 2012).